Hindawi
Advances in Civil Engineering
Volume 2019, Article ID 2973504, 12 pages
https://doi.org/10.1155/2019/2973504

Research Article

Simulation Study on the Dynamic Ventilation Control of Single Head Roadway in High-Altitude Mine Based on Thermal Comfort

Xingxin Nie,[1] **Shanshan Feng**,[2] **Zhang Shudu**,[2] **and Gan Quan**[1]

[1]*School of Resources Engineering, Xi'an University of Architecture and Technology, Xi'an 710055, Shaanxi, China*
[2]*School of Management, Xi'an University of Architecture and Technology, Xi'an 710055, Shaanxi, China*

Correspondence should be addressed to Xingxin Nie; 670127529@qq.com

Received 20 May 2019; Accepted 9 July 2019; Published 28 July 2019

Academic Editor: Yinshan Tang

Dynamic ventilation control based on the concept of thermal comfort is proposed and applied to single head roadway in high-altitude gold mine in Qinghai. Hourly thermal comfort values are determined for typical working conditions, and a thermal comfort curve is generated. The values are adjusted based on the external environment and the changes in the miners' thermal comfort. The Fluent software is used to simulate the temperature field and wind speed field of the tunnel roadway at three heights, and the results are used to fit the thermal comfort curve in the roadway. The results show that the thermal comfort is lowest at a roadway height of 1 m and a longitudinal length of 16 m because the wind speed is the highest and the temperature is lowest at these locations. When the dynamic ventilation control is used, the optimal thermal comfort levels can be determined for the locations in the single head roadway.

1. Introduction

The unique environment of high-altitude mines results in numerous mine ventilation issues such as low temperature, lack of oxygen, dryness, and poor ventilation. In the low-pressure, low-oxygen, low-humidity environment, the working efficiency of the ventilator is low, resulting in downhole ventilation. The low-oxygen underground environment also promotes the production of toxic and harmful gases. In particular, a large amount of toxic and harmful gases (carbon monoxide, sulfur dioxide, hydrogen sulfide, etc.) that are generated after blasting cannot be discharged in time and threaten the physical and mental health of miners [1–10]. Figure 1 shows a schematic diagram of ventilation monitoring for a gold mine in Qinghai [11, 12]. The ventilation monitoring system dynamically controls the downhole ventilation system through the use of sensors. The sensors include a wind pressure sensor, a wind speed sensor, and a fan opening and closing sensor. The wind speed sensors are located in the 4550 m return airway and the middle of each production stage. A wind speed alarm is set according to the standard; the main fan is equipped with a wind pressure sensor, and the measuring points are determined according to the requirements; the main fan has opening and closing sensors located near the ground. This traditional high-altitude mine ventilation monitoring data do not fully reflect the conditions in the downhole environment.

In this study, a dynamic ventilation control strategy based on the miners' thermal comfort is proposed; the method utilizes small regular fluctuations in a steady-state environment to achieve uniform thermal comfort and health while meeting the air quality requirements. The predicted mean vote (PMV), which predicts the average number of votes, is an indicator of the satisfaction of people with their environment, i.e, the thermal comfort. In general, there are six factors affecting the thermal comfort of miners, namely, air temperature, speed, relative humidity, ambient average radiant temperature, the metabolic rate of the body, and clothing thermal resistance. The PMV-predicted percentage

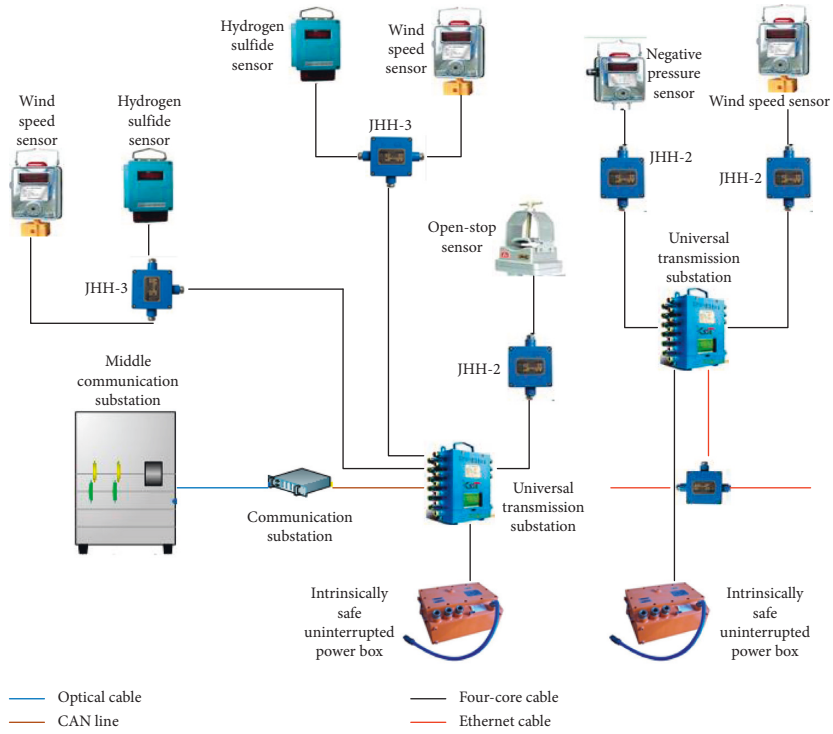

Figure 1: Schematic diagram of ventilation system monitoring equipment.

of dissatisfied (PPD) thermal comfort model is the earliest mathematical model of temperature regulation of the human body. The index used in this model indicates the average voting value of most people regarding the thermal environment. There are seven categories, namely, cold (−3), cool (−2), slightly cool (−1), neutral (0), slightly warm (1), warm (2), and hot (3). The research group of Professor Zhu of Tsinghua University conducted an experimental study on air conditioning, air supply dynamics, and human thermal comfort. The results showed that the user's thermal sensation was significantly better than the steady-state mode in the natural dynamic air supply mode [13, 14]. Duan and Li established thermal comfort indicators based on user preferences. By periodically adjusting the comfort zone and energy-saving zone to simulate the changes in the natural environment, the environmental health level was effectively improved [15, 16]. Zhang and Zhao discussed the effects of thermal sensation on the thermal comfort of a human body over time and space and established a thermal comfort model, which laid an important foundation for the study of comfort and energy conservation in unsteady environments [17, 18]. Zheng et al. analyzed and discussed the main influencing factors of human thermal comfort and pointed out that the value of human thermal comfort in the internal environments is composed of different factors [19]. However, the aforementioned studies failed to comprehensively consider the influence of the external thermal environment and the distribution of the temperature field and wind speed field in underground spaces when implementing dynamic ventilation control for optimum thermal comfort. In this study, the dynamic regulation of centralized air conditioning is applied to the dynamic regulation of the main ventilator of the mine. By considering the daily measured parameters of the thermal comfort of the uphole environment, the value of the thermal comfort of the downhole environment is simulated during the day and in each optimization cycle [20]. Numerical simulations are conducted in Fluent to investigate the temperature field and wind speed field at different heights of the underground roadway and to implement the dynamic regulation of the dynamic control of the underground roadway [21–24].

2. Establishment of PMV Model for High-Altitude Mine Workers

2.1. Correction of PMV Parameters in High-Altitude Mines

2.1.1. Correction of Convective Heat Transfer Parameters in Mines. Since most of the mine roadway is mechanically ventilated, people are exposed to forced convection air in the roadway; therefore, it is necessary to correct the convective heat transfer parameters of the mine. For example, equation (1) is the correlation of mine convective heat transfer [25–28]:

$$N_u = aR_e^n, \tag{1}$$

where N_u and R_e are the Nusselt number and Reynolds number, respectively; a and n are empirical constants, which are determined by using the commonly used convective heat transfer formula in the Fanger model; generally, 0.07 and 0.5 are used; ρ is the air density, kg·m^{-3}; v is the airflow velocity, m·s^{-1}; L is the height of the human body, m; and μ is the aerodynamic viscosity, i.e., 1.79×10^{-5} kg·m^{-1}·s^{-1}.

Due to the airflow velocity and air temperature at a given altitude, at a high altitude, the air density and atmospheric pressure in the mine are lower and it is necessary to correct the atmospheric pressure. Equation (2) is the relationship between the atmospheric pressure P_{ah} (kPa) at altitude H and the standard atmospheric pressure P_0 (kPa):

$$P_{ah} = P_0\left(1 - 2.257H \times 10^{-5}\right)^{5.526}. \quad (2)$$

Therefore, it can be concluded that the relationship between the convective heat transfer coefficient of the human body h_H ($W \cdot m^{-2} \cdot K^{-1}$) at different altitudes and the convective heat transfer coefficient of the human body h_0 ($W \cdot m^{-2} \cdot K^{-1}$) in the standard atmospheric environment is as follows:

$$h_H = h_0\left(1 - 2.257H \times 10^{-5}\right)^{5.526n}. \quad (3)$$

2.1.2. Correction of Evaporation Heat Transfer Coefficient of the Human Body. The evaporation heat transfer coefficient of the human body differs at different altitudes; therefore, it is necessary to adjust this coefficient to the high-altitude mine environment. The relationship between the evaporation heat transfer coefficient α_H ($W \cdot m^{-2} \cdot Pa^{-1}$) at altitude H and the evaporation heat transfer coefficient α_0 ($W \cdot m^{-2} \cdot Pa^{-1}$) in a standard atmospheric environment is as follows:

$$\alpha_H = \alpha_0\left(\frac{P_{ah}}{P_0}\right)^{n-1}. \quad (4)$$

We combine equations (2) and (4):

$$\alpha_H = \alpha_0\left(1 - 2.257H \times 10^{-5}\right)^{5.526(n-1)}. \quad (5)$$

2.1.3. Calculation of Metabolic Capacity. The human body produces heat when it performs certain activities, so the energy metabolism rate of the human body directly affects the heat exchange between the human body and the surrounding environment. The energy metabolism rate of the human body is affected by many factors, such as physical activity, special dynamic effects of things, age and gender, effects of climate and environmental temperature, malnutrition, and nervousness. Miners work in underground operations with high labor intensity and high metabolic rate, so the metabolic rate is an important indicator affecting the thermal comfort of miners. Equation (6) is the formula for calculating the metabolism of miners:

$$M = 352.2\left(\frac{0.233R_Q + 0.77V_{O_2}}{F_{D_u}}\right), \quad (6)$$

where R_Q is the respiratory coefficient, 0.83 ~ 1.0; V_{O_2} is the miners' oxygen consumption, L/min, 0.8 ~ 1.5 L/min is used in this study; and F_{D_u} is the surface area of the human body, m^2. For known values of the miner's height h (m) and weight m (kg), the formula for calculating the surface area of the human body is $F_{D_u} = 0.6h + 0.0128m - 0.1529$.

2.1.4. Heat Balance Equation and Thermal Comfort Index in Low-Altitude Environment. We substitute equations (3) and (5) into the heat balance equation [29] applicable to the low-pressure environment of high-altitude mines:

$$\begin{aligned} S = {} & M - W - S_a h_H (T_a - T_b) - \varepsilon_a S_a \varepsilon \sigma \left(T_a^4 - T_c^4\right) \\ & - 3.05 \times 10^{-3} (P_a - P_b) \frac{\alpha_H}{\alpha_0} - 0.42 (M - W - 58.15) \frac{\alpha_H}{\alpha_0} \\ & - 0.0014M (311 - T_a) \frac{h_H}{h_0} - 1.73 \times 10^{-5} (5867 - P_w) \frac{\alpha_H}{\alpha_0}, \end{aligned} \quad (7)$$

where S is the heat storage rate of the human body, W/m^2; M is the body's metabolic capacity, W/m^2; W is the number of joules produced by human work, W/m^2; S_a is the body's surface area coefficient; T_a is the average temperature of a clothed body, K; T_b is the air temperature, K; ε is the body's average radiance; ε_a is the effective radiation area coefficient of the body; σ is the radiation constant of the body, $\sigma = 5.7 \times 10^{-8}\ W \cdot m^{-2} K^{-4}$; T_c is the average radiant temperature of the environment, K; and P_a and P_b are the partial pressures of the saturated water vapor on the skin surface and the water vapor in the surrounding air, Pa.

The thermal comfort indicator PMV corrected for the high-altitude mine is defined in the following equation:

$$\text{PMV} = S(0.303e - 0.036M + 0.028). \quad (8)$$

The indicators used in this modified PMV model represent the average voting value of most people in this thermal environment. With regard to the aforementioned seven categories, PMV = 0 indicates that the indoor thermal environment is optimal for thermal comfort. The PMV value recommended in the standard ISO7730 is between −0.5 and +0.5. However, the general the calculation is based on PPD ≤20% and the corresponding PMV is in the range of −0.75 to +0.75.

2.2. Establishment of Downhole Thermal Comfort Model

2.2.1. Establishment of Adaptive Thermal Comfort Model. The downhole thermal comfort model is based on a simulation of the dynamic ventilation control. Richard developed an adaptive thermal comfort model for natural ventilation that was based on the meteorological characteristics of the external environment to establish an interior comfort zone [30]. In this study, an adaptive thermal comfort model of natural ventilation is established for the uphole and downhole environments in high-altitude areas. The model links the downhole neutral temperature with the average temperature in the well using linear regression [31]:

$$T_\theta = 17.8 + 0.31T_{\overline{x}}, \quad (9a)$$

where T_θ is the neutral temperature, °C; $T_{\overline{x}}$ is the average temperature in the well, °C.

Afterwards, Semin derived the relationship between the neutral temperature and the average temperature in high-altitude mine wells using the following equation:

$$T_\theta = 19.7 + 0.30T_{\overline{x}}. \quad (9b)$$

The thermal comfort evaluation model acceptable to 80% of users in the standard 55-1999 of the American Society of Heating, Refrigerating, and Air-Conditioning Engineers (ASHRAE) was used to determine the temperature range of high-altitude mines [32, 33].

The thermal comfort equation indicates that the airflow velocity is an important factor affecting the thermal comfort of the human body. Field experience and research have shown that natural ventilation is superior to mechanical ventilation in terms of comfort. Considering the influence of relative humidity and airflow speed on human thermal comfort, these factors are quantified, i.e., for a 10% increase in relative humidity, the temperature of the underground environment in a high-altitude mine increases by 0.4°C; for an increase in the wind speed of 0.15 of m/s, the temperature decreases by 0.55°C [34].

$$T_\theta = 19.7 + 0.30T_0 - (\varphi_0 - 70\%) + \frac{0.55v}{0.15}, \quad (9c)$$

where T_0 is the downhole temperature of the high-altitude mine, °C; φ_0 is the relative humidity of the well, % (when T_0 is greater than 28°C and φ_0 is less than 70%); and v is the wind speed, m/s. When T_0 is higher than 28°C, φ_0 has little effect on human thermal comfort and can be simplified to equation (9c).

2.2.2. Determination of Downhole Temperature and Wind Speed Setting. The meteorological data of the gold mine in Qinghai Province indicate that the annual average temperature is between 0.1°C and 0.8°C, the annual average maximum temperature is 12.2°C in July, the annual average minimum temperature is −11.6°C in January, the highest daily temperature is 28.1°C, and the lowest is −34.4°C. The average annual sunshine hours are 25084 h, the wind direction in winter and spring is from the northwest and the wind speed is 1~3 m/s, and the rainy season is June to September, accounting for 80% of the annual precipitation and the annual precipitation in the low mountain plain area ranges from 345.41 to 369.21 mm. The mining area has a dry cold continental climate characterized by dry and cold conditions, low rainfall, a short frost-free period, and large annual and diurnal temperature differences. The highest temperatures occur from May to September. Freezing temperatures occur from October to April. The minimum temperature is about −25°C. The rainy season ranges from July to August, and rainstorms and hail are common. The data used in this study are based on the climatic conditions at the gold mine in October, which has an effect on the temperature and wind speed data used in the PMV calculation. The measured data are compared with the expected value of the PMV to obtain the optimal temperature and wind speed values. The flow chart of the calculation process is shown in Figure 2.

In Figure 2, P_E is the expected value of PMV, T_0 is the temperature corresponding to P_E, v is the wind speed, T_a is the adjusted temperature increment, and the PMV measurement is the temperature T_0; φ_0 is the humidity, v is the measured wind speed of the internal environment based on the mathematical model, and T_c is the average radiant temperature; and the other parameters, the clothing thermal resistance, and the metabolic rates represent estimates that cannot be directly measured.

In order to achieve dynamic ventilation, it is necessary to adjust the parameters of the PMV based on the changes in the meteorological parameters of the well. We use a preset temperature value and compare the measured and expected PMV value (P_E). The PMV is inversely proportional to the temperature; therefore, if the PMV value is very large, it is necessary to reduce the set temperature value and vice versa. After the temperature set value is modified, we use the value and operate the circulation system and continue to compare the other indicators that affect the thermal comfort until the various parameter indicators meet the requirements.

3. Calculation and Analysis of Thermal Comfort Indicators for Workers at High Altitudes

3.1. Determination of Hourly Thermal Comfort Index of the Uphole Environment. There are large diurnal temperature differences in high-altitude areas, and the thermal comfort of underground workers is greatly affected by the environmental changes in the well. The concept of dynamic ventilation control is to control the thermal environment in the mine roadway by considering daily changes in the meteorological parameters. The climatic conditions of the gold mine in Qinghai Province are used as an example, and the real-time thermal comfort curve is established based on the predicted hourly temperature changes and other meteorological parameters in the gold mine.

3.1.1. Uphole Temperature Prediction. The hourly ambient temperature of the following day is predicted based on the highest and lowest temperature forecast by the meteorological department and the coefficient recommended by ASHRAE using the following formula:

$$T_\tau = T_h - \alpha_\tau (T_h - T_l), \quad (10)$$

where T_τ is the predicted value of the uphole environment at time τ, °C; α_τ is the predicted coefficient of the uphole environment at time τ; T_h is the historical highest temperature, °C; and T_l is the predicted temperature by the meteorological department based on the historical temperature, °C. The time-of-day prediction coefficient α_τ is shown in Table 1; the daily temperature changes in the well are represented by a sinusoidal curve.

For the test day, the highest temperature in the well is 5°C and the lowest temperature is −8°C. The ASHRAE coefficient method is used to predict the hourly dry-bulb temperature in the well. The results are shown in Table 2.

The prediction results show that from 0:00 am to 6:00 am, the temperature is decreasing, reaching the lowest value at 5:00 am. Subsequently, an upward trend is observed in the temperature until the highest value is reached

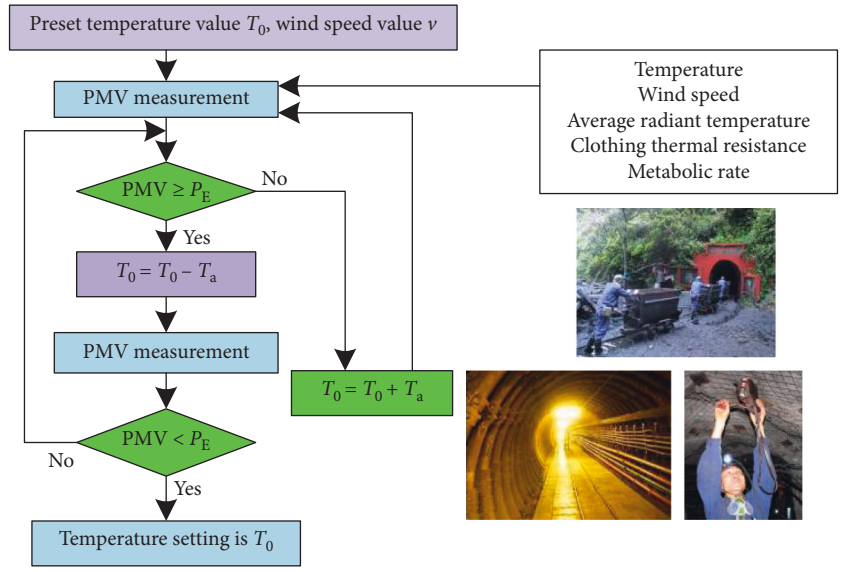

Figure 2: Flow chart for temperature and wind speed calculations.

Table 1: Uphole temperature prediction parameters.

Time	0	1	2	3	4	5	6	7	8	9	10	11
α_τ	0.82	0.87	0.92	0.96	0.99	1	0.98	0.93	0.84	0.71	0.56	0.39
Time	12	13	14	15	16	17	18	19	20	21	22	23
α_τ	0.23	0.11	0.03	0.00	0.03	0.10	0.21	0.34	0.47	0.58	0.68	0.76

Table 2: Predicted uphole temperatures.

Time	0	1	2	3	4	5	6	7	8	9	10	11
Temperature (°C)	−5.66	−6.31	−6.96	−7.48	−7.87	−8	−7.74	−7.09	−5.92	−4.23	−2.28	−0.07
Time	12	13	14	15	16	17	18	19	20	21	22	23
Temperature (°C)	2.01	3.57	4.61	5	4.61	3.7	2.27	0.58	−1.11	−2.54	−3.84	−4.88

at 15:00; then, the temperature gradually decreases from 4:00 pm to 11:00 pm. The highest and lowest temperatures are 5°C and −8°C.

3.1.2. Design Parameters for Thermal Comfort Adjustment in the Downhole Environment. PMV_{set} refers to the set value of the thermal comfort index. Research has shown that $PMV_{set} \in (-0.75, 0.75)$ is within the acceptable range of users [35], and this PMV index value was used in this study for the dynamic adjustment.

The predicted hourly thermal comfort values based on the proposed model are shown in Figure 3. The temperature and wind speed data for the gold mine from September to October were used. The thermal comfort value decreased from 0:00 to 5:00 and increased after 5:00. The thermal comfort value was relatively high from 12:00 to 18:00 and reached the maximum at 15:00. The predicted values were slightly lower than the measured values. The thermal comfort rating was cool from 7:00 to 11:00 and 19:00 to 2:00 and cold from 3:00 to 6:00.

3.2. Determination of Hourly Thermal Comfort Index of the Downhole Environment. The thermal comfort index is based on daily temperature. At high altitudes, the air is thin and oxygen-deficient, the temperature is low, and the PMV does not meet the standard value. The comfortable thermal evaluation of people in the uphole is cold, and the feeling of thermal comfort is also changing at different times. There is little change in the comfort index of the miners in the downhole environment during the day because the air volume and oxygen are not adjusted to increase the comfort level.

The proposed dynamic air supply strategy is as follows: first, the downhole thermal comfort control curve is developed. If the climatic conditions in the high-altitude area are harsh, the downhole comfort adjustment area is set to [−1, 1]. In the gold mine used in this example, the initial temperature and wind speed of the well are used. The optimization objective function is established to ensure that the downhole PMV value is as close as possible to the PMV value corresponding to the thermal comfort level of the miners while satisfying the constraints of the downhole temperature range, wind speed range, and PMV variation. The optimum

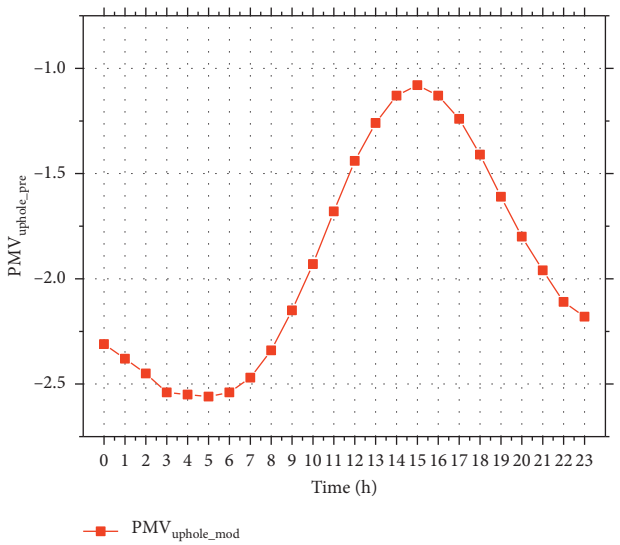

Figure 3: Predicted hourly thermal comfort data in the uphole environment.

temperature, humidity, wind speed, and other parameters values are obtained; each cycle lasts 4 h so that the comfort level fluctuates throughout the day and each cycle is in a relatively steady state. Figure 4 shows the flow chart of the downhole thermal comfort control strategy.

In Figure 4, t is the system time; $\mathrm{PMV}_{\mathrm{set}}$ is the thermal comfort index setting; $\mathrm{PMV}_{\mathrm{uphole}}$ is the uphole thermal comfort index; $\mathrm{PMV}_{\mathrm{downhole}}$ is the downhole thermal comfort index; $\mathrm{PMV}_{\mathrm{uphole\_pre}}$ is the uphole hourly weather prediction curve; $\mathrm{PMV}_{\mathrm{uphole\_mod}}$ is the uphole hourly thermal comfort correction curve; T_{initial} is the initial temperature setting; V_{initial} is the initial wind speed; T_{downhole} is the downhole temperature setting; V_{downhole} is the downhole wind speed; $\Delta T_{\mathrm{downhole}}$ is the downhole temperature change; $\Delta\mathrm{PMV}_{\mathrm{downhole}}$ is the PMV change; Ω is the set of comfort domains; J_{pmv} is the steady-state temperature field—the wind speed field; $T(x, y, z)$ is the temperature at the coordinate (x, y, z); and $V(x, y, z)$ is the wind speed at the coordinate (x, y, z).

The value of the clothing thermal resistance used in the calculation is 1, which is the standard value of the clothing thermal resistance of the human body in winter. In order to generate the downhole thermal comfort curve that meets the requirements of the human body, the hourly thermal comfort value of the well is optimized. The clothing thermal resistance is increased to approach the standard value of thermal comfort. As shown in Figure 5, the corrected curve of the downhole thermal comfort is based on the thermal comfort prediction curve and the parameters were modified. The results indicate that the human thermal comfort standard is met. The thermal comfort indices from 0:00 to 11:00 and 18:00 to 23:00 were hot and neutral and slightly warm from 12:00 to 13:00. Figure 6 shows the contrast curve between the uphole and downhole thermal comfort. The red curve is the measured trend of thermal comfort on the well. The blue curve is the trend of thermal comfort annotation after optimization. The optimized thermal comfort changes are evident from Figure 6.

4. Numerical Simulation of Dynamic Ventilation Control of a Single Roadway

4.1. Physical Model and Mesh Division of a Single Roadway. The three-dimensional physical model of the design of the single roadway in the gold mine in Qinghai Province is shown in Figure 7. The length of the roadway is 25 m and the height is 3 m. The air duct is located in the middle of the roof of the roadway. The length of the air duct is 10 m and the radius is 0.15 m [36–43]. Figure 7(a) shows the inlet cross-sectional view of the single roadway, Figure 7(b) is the three-dimensional model of the roadway, Figure 7(c) is the internal space of the three-dimensional roadway, and Figure 7(d) is the longitudinal section of the roadway. In order to facilitate the calculation, a two-dimensional model of the midplane from the exit of the air duct to the end of the roadway is intercepted, and the numerical simulation of the temperature field and the wind speed field is conducted for the single roadway. The design uses press-in ventilation, and the air duct enters the roadway. The air volume is 10 m/s [44]. The model is meshed using the ICEM CFD 19.0 software, as shown in Figure 7(e).

4.2. Setting of Boundary Conditions and Initial Conditions in Fluent. (1) The model inlet, i.e., the outlet temperature of the air duct is set to $T = 296$ K, and the inlet wind speed is $v = 10$ m/s. The inlet boundary in the numerical model is the outlet of the forced fan, and the boundary type is the velocity inlet; (2) at the roadway exit, pressure $P = 0$ is applied and the boundary condition is the outflow; (3) the temperatures of the air cylinder wall boundary, the roadway wall boundary, and the roadway surface are 300 K, 305 K, and 308 K, respectively; and (4) the wall surface has no-slip boundary conditions. The wind speed at the wall is 0 m/s, and the standard wall function method is used [45, 46].

4.3. Numerical Simulation Results. Figure 8 shows the distribution of the wind flow velocity vector in the mine roadway. The wind flow consists of the jet zone, the recirculation zone, and the vortex zone. The uppermost red area is the inlet of the air duct. After the forced air enters the roadway, it flows along the roadway in free jet flow mode. Then, it is reflected by the wall and flows opposite to the jet direction, forming a vortex, as shown in the middle part of the figure; another portion of the flow is directed along the roadway.

In order to investigate the wind speed at different heights of the roadway, the wind speed was measured at three heights in the roadway (1 m, 1.5 m, and 2 m). Figure 9 shows the wind velocity at the three positions. After the forced air from the air duct enters the roadway, the wind speed begins to rise rapidly and then decreases in the middle of the roadway. The reason is that the vortex flow rate is small due to eddy currents; the wind speed is lowest at $y = 1.5$ m.

Figure 10 shows the temperature in the roadway during forced ventilation. The temperature is measured at the same three heights. The temperature of the roadway is relatively uniform. Figure 11 shows the temperature at the three

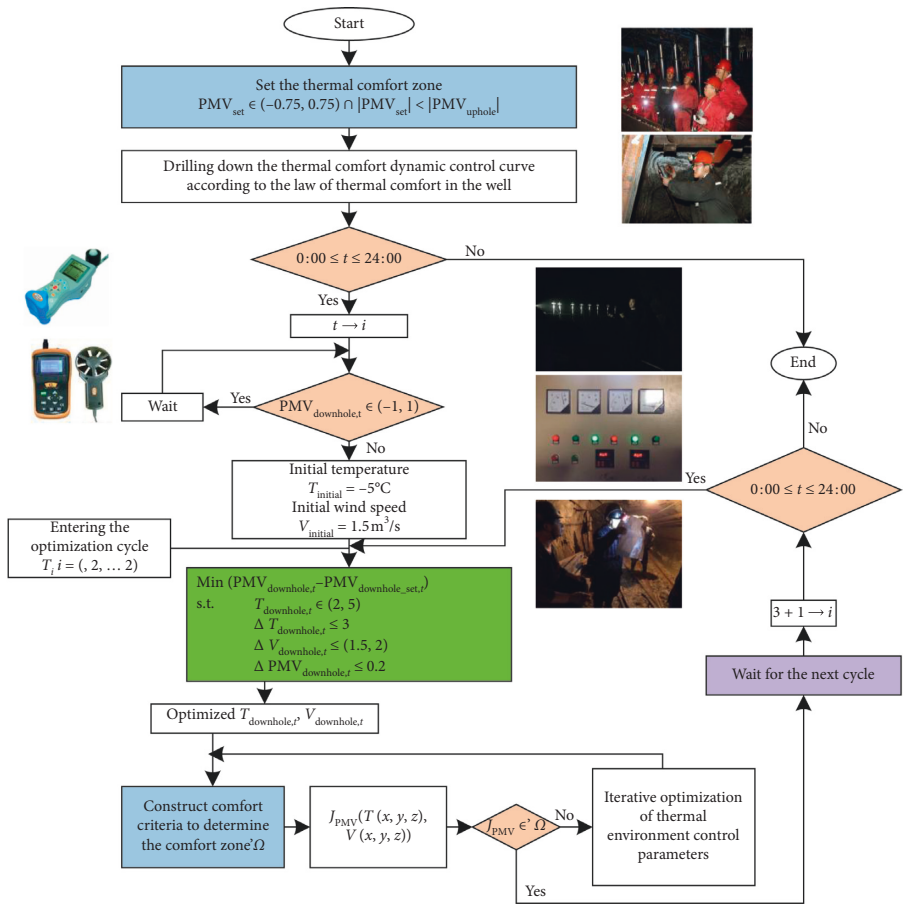

Figure 4: Dynamic flow compensation strategy to obtain the optimal comfort level in mines in high-altitude areas.

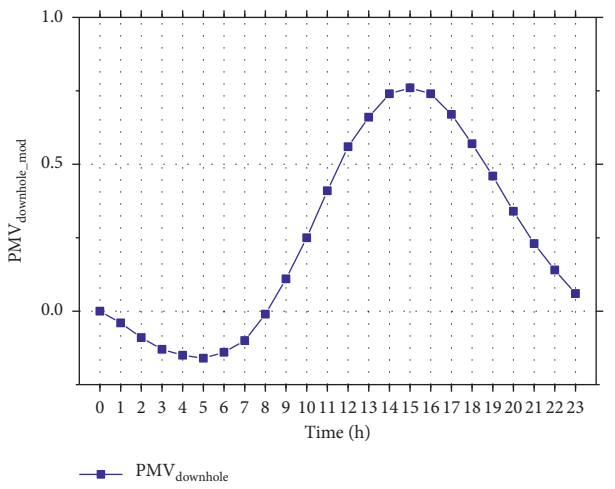

Figure 5: Downhole thermal comfort based on dynamic regulation. Note: PMV_{uphole_pre} refers to the predicted thermal comfort values in the well; $PMV_{downhole\_mod}$ refers to the modified downhole thermal comfort values; and PMV refers to the difference between the conditions in the well and the downhole thermal comfort.

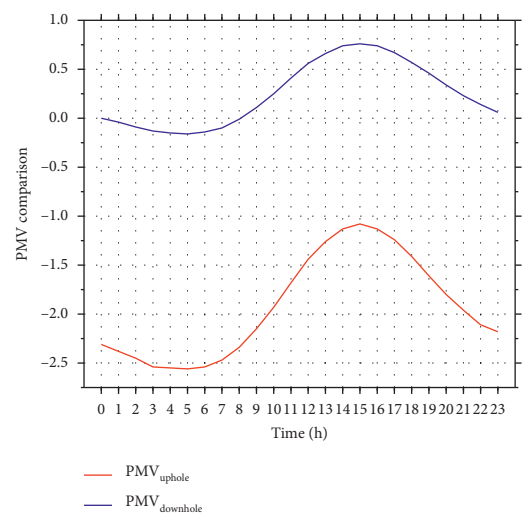

Figure 6: Thermal comfort curves in the uphole and downhole environments. Note: PMV_{uphole_pre} refers to the predicted thermal comfort values in the well; $PMV_{downhole\_mod}$ refers to the modified downhole thermal comfort values; and PMV refers to the difference between the conditions in the well and the downhole thermal comfort.

heights of the roadway. The temperature is similar but a very low value is obtained in the vortex area of the roadway. The ventilation efficiency is low, and the temperature is high.

4.4. Ventilation Dynamic Control and Effect Analysis. The thermal comfort analysis of the environment indicates that temperature and wind speed are the dominant factors

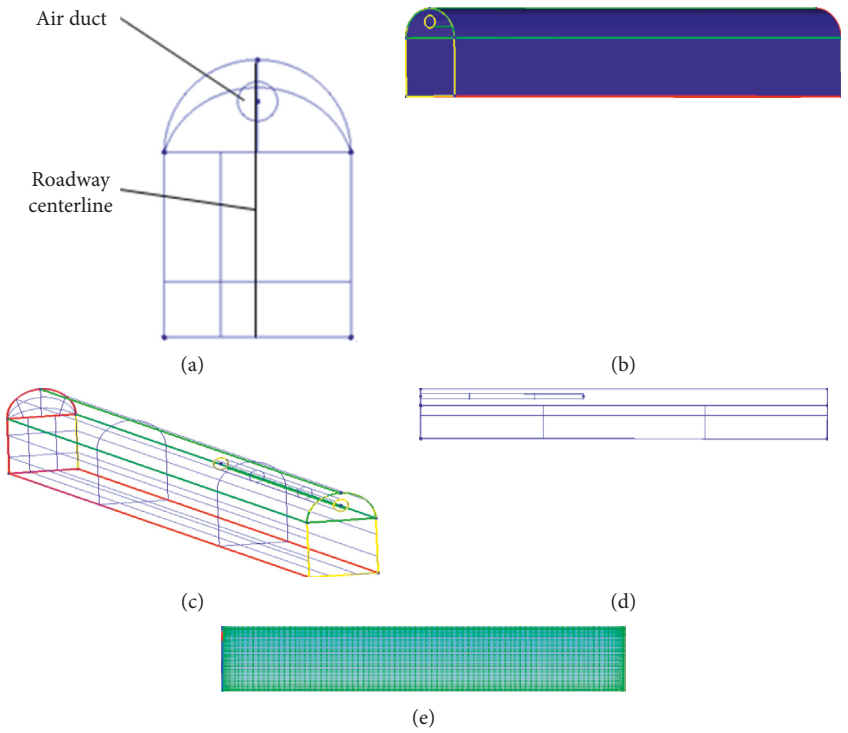

Figure 7: Three-dimensional model of a single roadway. (a) Entrance cross section. (b) 3D model diagram. (c) Unfilled color 3D model diagram. (d) Longitudinal section of roadway. (e) Mesh map. Note: the red part on the left side of Figure 7(e) is the inlet of the air duct, and the blue part is the exit area of the single roadway.

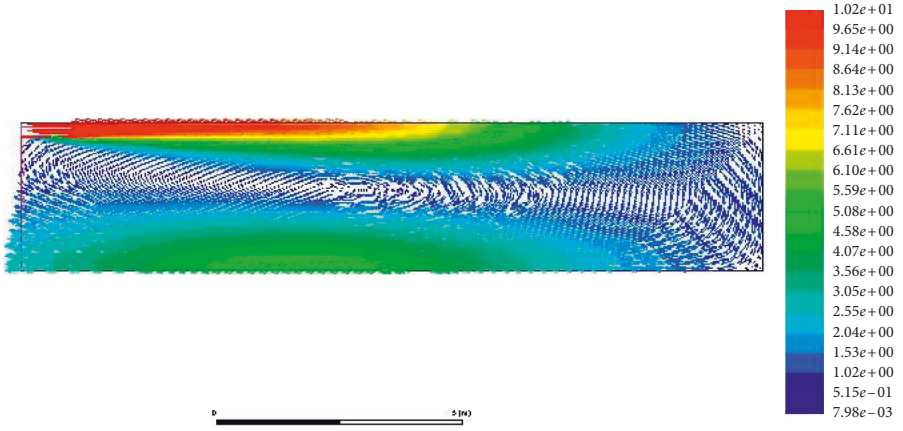

Figure 8: Wind flow velocity vector.

affecting the thermal comfort of the body. The PMV values at different heights of the roadway are determined using MATLAB software and the numerical simulation results of the temperature field and the wind speed field [47–52]. As shown in Figure 12, the PMV values are in the range of −0.6~0.6, conforming to the standard value of human thermal comfort. The PMV results predict slightly cooler conditions at a distance of 12 m to 19 m, and the value is lowest at 16 m. The numerical simulation results demonstrate that the temperature is relatively uniform in this range, and the wind speed is relatively high; therefore, the PMV value is relatively low. Therefore, the feedback parameters of the dynamic air supply compensation strategy are based on the values at $x = 16$ m and $y = 1$ m.

5. Conclusions

The thermal comfort theory is applied to the dynamic ventilation control of mines in high-altitude areas by considering the unique climatic characteristics and environmental conditions of high-altitude mines. The CFD software Fluent is used to conduct numerical simulation tests on the underground tunnels. The results lead to the following conclusions:

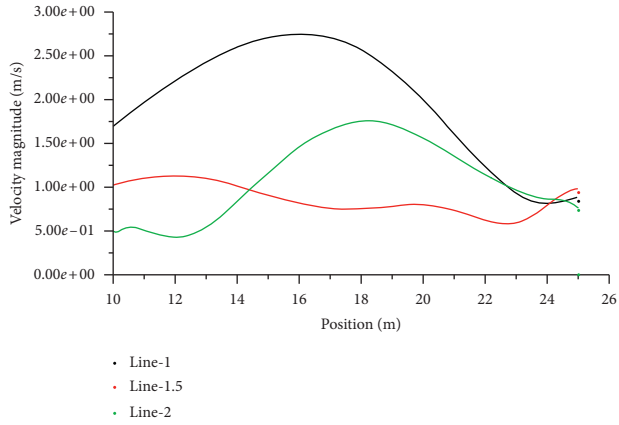

Figure 9: Wind speed at three heights in the roadway.

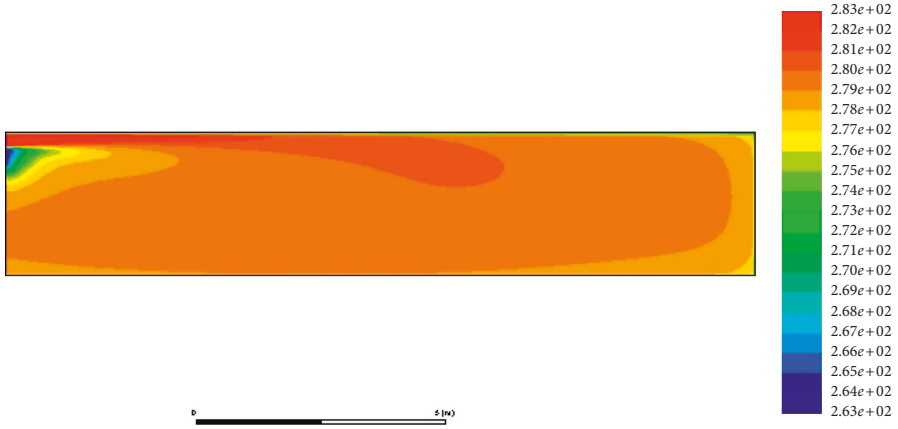

Figure 10: Temperature in the roadway during forced ventilation.

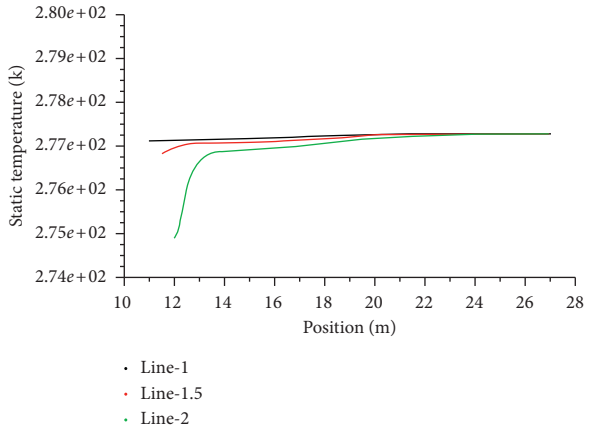

Figure 11: Temperature at three heights in the roadway.

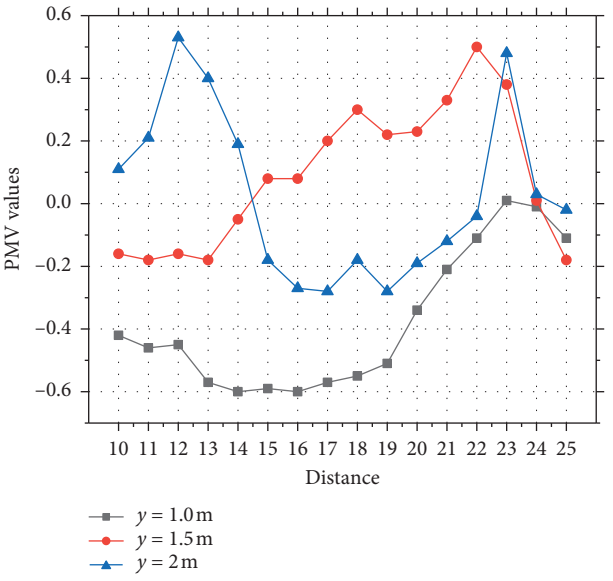

Figure 12: PMV values at different heights of the roadway.

(1) The ventilation conditions of mines in high-altitude areas are inadequate, and the PMV values in underground mines are significantly affected by the

environment in the well. Therefore, PMV indicators applicable to mines located in low lying areas are not applicable to high-altitude mines. We used meteorological data for a gold mine in Qinghai to predict the hourly thermal comfort levels in the downhole environment and to assess the changes in the thermal comfort of the underground workers during the day.

(2) Numerical simulations of the temperature field and wind speed field were conducted at different heights of the underground roadway, and the data were used to predict the thermal comfort degree in the underground environment at different locations.

(3) The proposed dynamic ventilation control strategy for the high-altitude mine based on the downhole thermal comfort comprehensively considers the advantages of natural ventilation and the conditions at different heights of the underground roadway to ensure the comfort of people in the underground environment and reduce energy consumption. The results of this study provide important theoretical guidance. However, we only conducted a simulation of single roadway, and the influence of changes in the air supply parameters on multiple roadways requires further study.

Data Availability

The experimental data used in this study were obtained from the Manzhanggang Gold Mine in Qinghai Province, China. There are two main sources of thermal comfort data: one is the historical meteorological parameters of the Meteorological Bureau, and the other is the temperature, wind speed, and humidity of the typical conditions of the gold mine from September to October. The dynamic ventilation control of the single-head roadway in high-altitude mine based on thermal comfort can be applied to underground mines with similar problems. Data used to support the results of this study can be obtained from the corresponding author.

Conflicts of Interest

The authors declare no conflicts of interest.

Authors' Contributions

Xingxin Nie contributed to conceptualization, methodology, analysis using software, and formal analysis; Shanshan Feng was responsible for investigation, data curation, and writing; Zhang Shudu visualized the study; and Zhang Shudu and Gan Quan supervised the study.

Acknowledgments

This work was supported by the Social Science Foundation of Shaanxi Province, China (2018S12), and Natural Science Foundation of Shaanxi Province, China (2016JM5088).

References

[1] C. A. Almaz, A. M. Sartmyrzaeva, M. Abdirashit et al., "High altitude pulmonary edema in a mining worker with an abnormal rise in pulmonary artery pressure in response to acute hypoxia without prior history of high altitude pulmonary Edema," *Wilderness and Environmental Medicine*, vol. 28, no. 3, pp. 234–238, 2017.

[2] J. Lai, X. Wang, J. Qiu et al., "A state-of-the-art review of sustainable energy based freeze proof technology for cold-region tunnels in China," *Renewable and Sustainable Energy Reviews*, vol. 82, pp. 3554–3569, 2018.

[3] X. X. Nie, W. J. Zhai, and C. W. Lu, "Price prediction of molybdenum concentrate based on grey-markov model," *Journal of Environmental Protection and Ecology*, vol. 19, no. 4, pp. 1955–1963, 2018.

[4] Y. M. Zhang, S. Q. He, G. Q. Li, and N. L. Hu, "Optimization of ventilation system in plateau mine based on ventsim," *China Mining Industry*, vol. 25, no. 7, pp. 82–86, 2016.

[5] X. D. Wang, *Research on Mine Ventilation System in High Altitude Metal Mines*, University of Science and Technology Beijing, Beijing, China, 2015.

[6] Y. H. Cui, *Influence of Plateau Low Pressure Environment on Mine Safety Production and Countermeasures*, Shandong University of Science and Technology, Qingdao, China, 2010.

[7] Q. R. Cao and K. Li, "Study on the influence of managerial behavior on unsafe behavior of miners," *Journal of Management Science*, vol. 24, no. 6, pp. 69–78, 2011.

[8] E. J. Haas and M. Mattson, "A qualitative comparison of susceptibility and behavior in recreational and occupational risk environments: implications for promoting health and safety," *Journal of Health Communication*, vol. 21, no. 6, pp. 705–713, 2016.

[9] G. J. Fogarty and A. Shaw, "Safety climate and the theory of planned behavior: towards the prediction of unsafe behavior," *Accident Analysis and Prevention*, vol. 42, no. 5, pp. 1455–1459, 2010.

[10] W. Xiao, Y. Zhao, J. Yang et al., "Effect of sodium oleate on the adsorption morphology and mechanism of nanobubbles on the mica surface," *Langmuir*, 2019.

[11] J. L. Qiu, Y. W. Qin, J. Lai et al., "Structural response of the metro tunnel under local dynamic water environment in loess strata," *Geofluids*, vol. 2019, Article ID 8541959, 16 pages, 2019.

[12] X. Nie, X. Wei, X. Li, and C. Lu, "Heat treatment and ventilation optimization in a deep mine," *Advances in Civil Engineering*, vol. 2018, Article ID 1529490, 12 pages, 2018.

[13] W. J. Ji, M. H. Luo, B. Cao, and Y. X. Zhu, "Study on the influence of long-term thermal experience on thermal comfort evaluation and thermal adaptability," *HVAC*, vol. 48, no. 1, pp. 78–82, 2018.

[14] M. H. Luo, J. Yu, Y. T. Yang, and Y. X. Zhu, "Experimental study on air conditioning dynamics and human thermal comfort in split air conditioning under isothermal conditions," *HVAC*, vol. 44, no. 5, pp. 130–134, 2014.

[15] P. Y. Duan, C. C. Liu, C. X. Duan, and H. Li, "Indoor dynamic thermal comfort control method based on particle swarm optimization," *Information and Control*, vol. 42, no. 1, pp. 100–110, 2013.

[16] X. Feng, P. Y. Dua, and C. X. Duan, "Design of indoor environmental thermal comfort controller based on PMV index," *Shandong Science*, vol. 29, no. 1, pp. 110–115, 2016.

[17] Y. F. Zhang and R. Y. Zhao, "Review and discussion on research on human body thermal adaptation in building environment," *HVAC*, vol. 40, no. 9, pp. 38–48, 2010.

[18] Y. Zhang and R. Zhao, "Relationship between thermal sensation and comfort in non-uniform and dynamic environments," *Building and Environment*, vol. 44, no. 7, pp. 1386–1391, 2009.

[19] H. F. Zheng, Y. H. Liang, X. W. Fan, and G. J. Tian, "Analysis of influencing factors of indoor dynamic thermal comfort," *Journal of Thermal Science and Technology*, vol. 14, no. 4, pp. 259–266, 2015.

[20] Y. Liu, Y. Xiao, J. Chen, G. Augenbroe, and T. Zhou, "A network model for natural ventilation simulation in deep buried underground structures," *Building and Environment*, vol. 153, pp. 288–301, 2019.

[21] C. Ding, X. Q. He, and B. S. Nie, "Numerical simulation of airflow distribution in mine tunnels," *International Journal of Mining Science and Technology*, vol. 27, no. 4, pp. 663–667, 2017.

[22] Y. Liu, S. Wang, Y. Ma, Y. Deng, and W. Ma, "Numerical simulation and experimental study on ventilation system for powerhouses of deep underground hydropower stations," *Applied Thermal Engineering*, vol. 105, pp. 151–158, 2016.

[23] Y. Xia, D. Yang, C. Hu, C. Wu, and J. Han, "Numerical simulation of ventilation and dust suppression system for open-type TBM tunneling work area," *Tunnelling and Underground Space Technology*, vol. 56, pp. 70–78, 2016.

[24] G. Xu, K. D. Luxbacher, S. Ragab, and S. Schafrik, "Development of a remote analysis method for underground ventilation systems using tracer gas and CFD in a simplified laboratory apparatus," *Tunnelling and Underground Space Technology*, vol. 33, pp. 1–11, 2013.

[25] Y. Nishi and A. P. Gagge, "Direct evaluation of convective heat transfer coefficient by napthalene sublimation," *Journal of Applied Physiology*, vol. 29, no. 6, pp. 830–838, 2013.

[26] R. E. Treybal, *Mass Transfer Operations*, McGraw-Hill, New York, NY, USA, 2013.

[27] M. A. Semin and L. Y. Levin, "Stability of air flows in mine ventilation networks," *Process Safety and Environmental Protection*, vol. 124, pp. 167–171, 2019.

[28] P. Roghanchi, K. C. Kocsis, and M. Sunkpal, "Sensitivity analysis of the effect of airflow velocity on the thermal comfort in underground mines," *Journal of Sustainable Mining*, vol. 15, no. 4, pp. 175–180, 2016.

[29] N. Chen, S. M. Liao, and Z. H. Rao, "CFD evaluation of temperature field and thermal comfort of low-pressure aerobic passenger trains," *China Railway Science*, vol. 33, no. 4, pp. 126–132, 2012.

[30] R. J. de Dear and G. S. Brager, "Thermal comfort in naturally ventilated buildings: revisions to ASHRAE Standard 55," *Energy and Buildings*, vol. 34, no. 6, pp. 549–561, 2012.

[31] H. Zhang, E. Arens, and Y. C. Zhai, "A review of the corrective power of personal comfort systems in non-neutral ambient environments," *Building and Environment*, vol. 91, pp. 15–41, 2015.

[32] L. Yang, *Research on Building Climate Analysis and Design Strategy*, Xi'an University of Architecture and Technology, Xi'an, China, 2003.

[33] V. F. Ličina, T. Cheung, H. Zhang et al., "Development of the ASHRAE global thermal comfort database II," *Building and Environment*, vol. 142, pp. 502–512, 2018.

[34] M. L. Duan, X. W. Sun, X. L. Li, Z. H. Wang, and Z. Q. Qi, "Relationship between human thermal comfort and indoor thermal environment parameters in various regions of China (continued)," *Architecture Science*, vol. 34, no. 12, pp. 114–120, 2018.

[35] L. Jie, Y. Peng, and L. Wensheng, "Safety entropy research of working environment parameters in plateau non-coal underground mine," *Procedia Engineering*, vol. 43, pp. 197–203, 2012.

[36] J. Lai, S. Mao, J. Qiu et al., "Investigation progresses and applications of fractional derivative model in geotechnical engineering," *Mathematical Problems in Engineering*, vol. 2016, pp. 1–15, 2016.

[37] H. Sun, Q. P. Wang, P. Zhang, Y. J. Zhong, and X. B. Yue, "Spatiotemporal characteristics of tunnel traffic accidents in China from 2001 to present," *Advances in Civil Engineering*, vol. 2019, Article ID 4536414, 16 pages, 2019.

[38] M. Bahaaddini, G. Sharrock, and B. K. Hebblewhite, "Numerical investigation of the effect of joint geometrical parameters on the mechanical properties of a non-persistent jointed rock mass under uniaxial compression," *Computers and Geotechnics*, vol. 49, pp. 206–225, 2013.

[39] S. Y. Liu, L. T. Shao, and H. J. Li, "Slope stability analysis using the limit equilibrium method and two finite element methods," *Computers and Geotechnics*, vol. 63, pp. 291–298, 2015.

[40] Q. Wang and H. Sun, "Traffic structure optimization in historic districts based on green transportation and sustainable development concept," *Advances in Civil Engineering*, vol. 2019, Article ID 9196263, 18 pages, 2019.

[41] J. Qiu, T. Yang, X. Wang, L. Wang, and G. Zhang, "Review of the flame retardancy on highway tunnel asphalt pavement," *Construction and Building Materials*, vol. 195, pp. 468–482, 2019.

[42] J. Qiu, Y. Qin, Z. Feng, L. Wang, and K. Wang, "Safety risks and protection measures for the city wall during the construction and operation of Xi'an metro," *Journal of Performance of Constructed Facilities*, vol. 33, no. 5, p. 12, 2019.

[43] J. L. Qiu, H. Q. Liu, J. X. Lai, H. P. Lai, J. X. Chen, and K. Wang, "Investigating the long-term settlement of a tunnel built over improved loessial foundation soil using jet grouting technique," *Journal of Performance of Constructed Facilities*, vol. 32, no. 5, article 04018066, 2018.

[44] J. Qiu, X. Wang, J. Lai, Q. Zhang, and J. Wang, "Response characteristics and preventions for seismic subsidence of loess in Northwest China," *Natural Hazards*, vol. 92, no. 3, pp. 1909–1935, 2018.

[45] J. Lai, X. Wang, J. Qiu, J. Chen, Z. Hu, and H. Wang, "Extreme deformation characteristics and countermeasures for a tunnel in difficult grounds in southern Shaanxi, China," *Environmental Earth Sciences*, vol. 77, no. 19, p. 706, 2018.

[46] L. Duan, Y. Zhang, and J. Lai, "Influence of ground temperature on shotcrete-to-rock adhesion in tunnels," *Advances in Materials Science and Engineering*, vol. 2019, Article ID 8709087, 18 pages, 2019.

[47] Q. Liu, X.-B. Feng, Y.-L. He, C.-W. Lu, and Q.-H. Gu, "Multiple-relaxation-time lattice Boltzmann model for simulating axisymmetric thermal flows in porous media," *International Journal of Heat and Mass Transfer*, vol. 137, pp. 1301–1311, 2019.

[48] G. P. Liu, "Analysis of the heat returning from roadway and its influencing factors," *Mining Safety and Environmental Protection*, vol. 45, no. 6, pp. 10–14, 2018.

[49] C. Wang, G. Wu, and G. Wang, "Study on parametric and numerical simulation of local forced ventilation," *Procedia Engineering*, vol. 45, pp. 786–792, 2012.

[50] F. Geng, G. Luo, Y. Wang et al., "Dust dispersion in a coal roadway driven by a hybrid ventilation system: a numerical

study," *Process Safety and Environmental Protection*, vol. 113, pp. 388–400, 2018.

[51] H. B. Xie, D. B. Zhang, and L. C. Shen, "Research on co-simulation method based on matlab/simulink and fluent," *Journal of System Simulation*, vol. 8, pp. 1824–1856, 2007.

[52] S. S. Wu, J. P. Guo, G. B. Shi, J. P. Li, and C. W. Lu, "Laboratory-based investigation into stress corrosion cracking of cable bolts," *Materials*, vol. 12, no. 13, 2019.